The RhoE/ROCK/ARHGAP25 signaling pathway controls cell invasion by inhibition of Rac activity

Sylvie Thuault[a,*,†], Franck Comunale[a], Jessy Hasna[a,‡], Mathieu Fortier[a,§], Damien Planchon[a], Nabila Elarouci[b], Aurélien De Reynies[b], Stéphane Bodin[a], Anne Blangy[a], and Cécile Gauthier-Rouvière[a,*]
[a]Université de Montpellier, CRBM, CNRS, UMR 5237, 34293 Montpellier, France; [b]Ligue Nationale Contre le Cancer, Cartes d'Identité des Tumeurs, 75013 Paris, France

ABSTRACT **Rhabdomyosarcoma (RMS) is the most common soft tissue sarcoma of skeletal muscle origin in children and adolescents. Among RMS subtypes, alveolar rhabdomyosarcoma (ARMS), which is characterized by the presence of the PAX3-FOXO1A or PAX7-FOXO1A chimeric oncogenic transcription factor, is associated with poor prognosis and a strong risk of metastasis compared with the embryonal subtype (ERMS). To identify molecular pathways involved in ARMS aggressiveness, we first characterized the migratory behavior of cell lines derived from ARMS and ERMS biopsies using a three-dimensional spheroid cell invasion assay. ARMS cells were more invasive than ERMS cells and adopted an ellipsoidal morphology to efficiently invade the extracellular matrix. Moreover, the invasive potential of ARMS cells depended on ROCK activity, which is regulated by the GTPase RhoE. Specifically, RhoE expression was low in ARMS biopsies, and its overexpression in ARMS cells reduced their invasion potential. Conversely, ARHGAP25, a GTPase-activating protein for Rac, was up-regulated in ARMS biopsies. Moreover, we found that ARHGAP25 inhibits Rac activity downstream of ROCKII and is required for ARMS cell invasion. Our results indicate that the RhoE/ROCK/ARHGAP25 signaling pathway promotes ARMS invasive potential and identify these proteins as potential therapeutic targets for ARMS treatment.**

Monitoring Editor
Jonathan Chernoff
Fox Chase Cancer Center

Received: Jan 19, 2016
Revised: Jul 5, 2016
Accepted: Jul 6, 2016

INTRODUCTION

Rhabdomyosarcoma (RMS) is the most common soft tissue sarcoma in children and adolescents (Merlino and Helman, 1999). Two major types of RMS with different outcomes exist: the alveolar subtype (ARMS) is more aggressive than the embryonal subtype (ERMS) and often displays widespread metastases and resistance to conventional chemotherapy and radiotherapy, resulting in a 5-yr survival rate of only 30% (Breneman *et al.*, 2003). Whereas no consistent and specific genetic alterations have been identified in ERMS, ARMS is characterized by a reciprocal translocation that results in the production of the PAX3-FOXO1A or PAX7-FOXO1A fusion protein, which consists of the N-terminal PAX3/PAX7 DNA-binding domain and the C-terminus of the transactivation domain of FOXO1A, a member of the forkhead/HNF-3 transcription factor family (Barr, 2001). A translocation that generates a fusion protein composed of PAX3 and the nuclear receptor coactivator NCOA1 was also described (Wachtel *et al.*, 2004). Fusion-positive ARMS has the worse prognosis of RMS (Sorensen *et al.*, 2002; Williamson *et al.*, 2010). Indeed, RMS cases histologically classified as ARMS but that do not contain the fusion gene PAX3/7-FOXO1A are indistinguishable from ERMS cases (Williamson *et al.*, 2010). There is no specific therapeutic strategy against ARMS, and therefore it is crucial to identify new molecular targets.

Cell migration and invasion are key processes involved in cancer cell dissemination and metastasis. Cancer cells can use different mechanisms to invade through the extracellular matrix (ECM), depending on adhesion, actomyosin contractility, small Rho GTPases, and ECM composition. Cells can migrate collectively by keeping cell–cell contacts or individually (Friedl and Wolf, 2010; Friedl and Alexander, 2011; Sanz-Moreno and Marshall, 2010). When migrating

This article was published online ahead of print in MBoC in Press (http://www.molbiolcell.org/cgi/doi/10.1091/mbc.E16-01-0041) on July 13, 2016.

Present addresses: [†]CRCM, Inserm, U1068; Institut Paoli-Calmettes; Aix-Marseille Université, UM 105; CNRS, UMR7258; 13009 Marseille, France; [‡]University of Picardie Jules Verne, UFR Sciences, EA 4667, Laboratory of Cell and Molecular Physiology, SFR CAP-SANTE (FED 4231), Amiens, France; [§]Institut de Génomique Fonctionnelle, 34094 Montpellier Cedex 05, France.

*Address correspondence to: Sylvie Thuault (sylvie.thuault@inserm.fr), Cécile Gauthier-Rouvière (cecile.gauthier@crbm.cnrs.fr).

Abbreviations used: ARMS, alveolar rhabdomyosarcoma; ARMSfn, fusion-negative ARMS; ARMSfp, fusion-positive ARMS; 3D, three-dimensional; ECM, extracellular matrix; ERMS, embryonal rhabdomyosarcoma; GAP, GTPase-activating protein; GFP, green fluorescent protein.

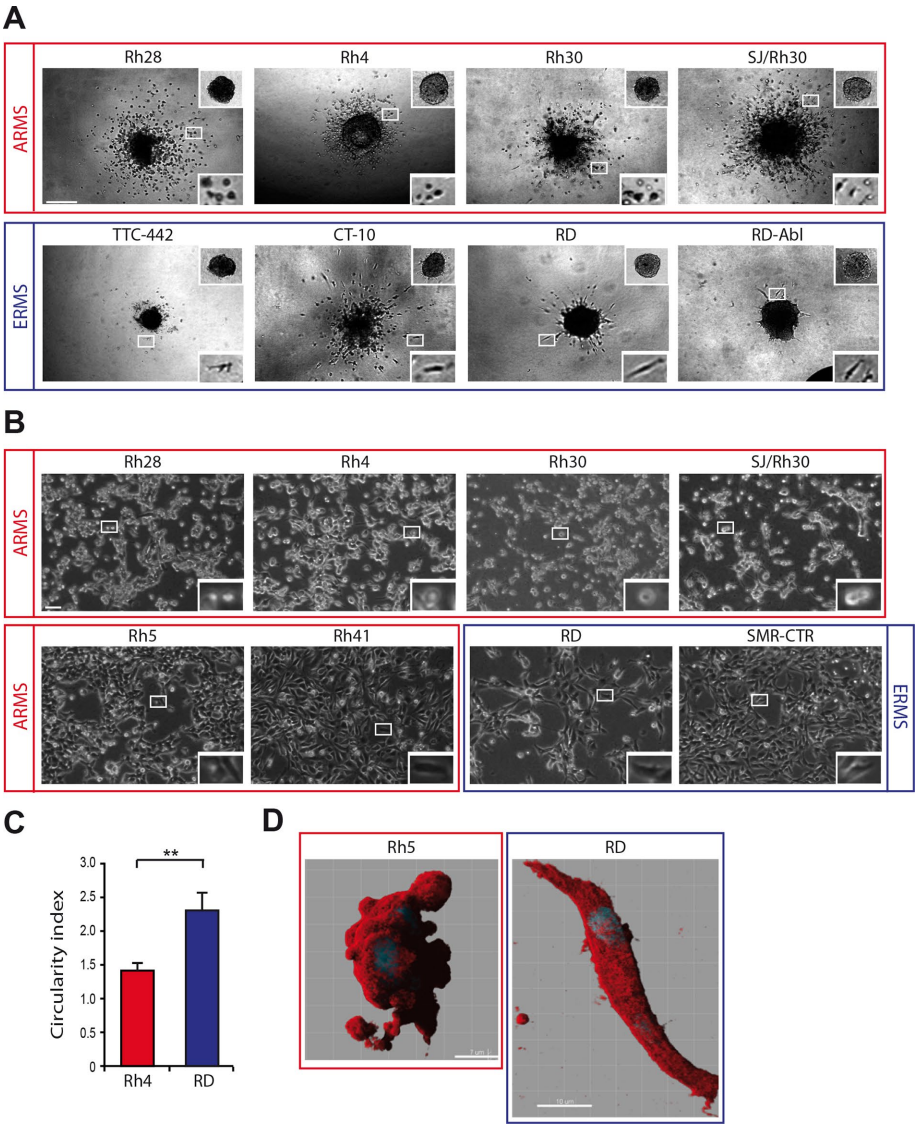

FIGURE 1: ARMS cell lines are more invasive than ERMS cell lines and adopt a rounded morphology during invasion through type I collagen matrix. (A) Phase-contrast images of spheroids formed using different ARMS and ERMS cell lines embedded in a 3D type I collagen matrix for 2 d. The upper insets show spheroids at day 0 just after embedding. The boxed regions are shown enlarged in the bottom insets. Images are representative of at least 20 spheroids analyzed in three independent experiments. Bar, 200 µm. (B) Phase-contrast photographs of ARMS and ERMS cell lines seeded on top of a thick, deformable layer of type I collagen. The boxed regions are shown enlarged in the insets. Bar, 50 µm. (C) Analysis of cell morphology by calculating the reciprocal of the circularity index (perimeter^2/4π × area) of cells from the experiment described in B; mean ± SD of one representative ERMS (RD) and ARMS (Rh4) cell line (**$p < 0.01$). (D) Cell morphology after 3D reconstitution of confocal images of Rh5 (ARMS) and RD (ERMS) cells during invasion in type I collagen matrix after staining with rhodamine-conjugated phalloidin (red; actin cytoskeleton) and Hoechst (blue; nuclei). Bar, 7 µm (Rh5 cells), 10 µm (RD cells).

individually in three-dimensional (3D) matrices, cells display two main motility modes (Friedl and Wolf, 2010). The mesenchymal mode is characterized by an elongated cell morphology with strong cell–substrate adhesion, prominent actin stress fibers, and actin-rich protrusions, including lamellipodia and filopodia. During amoeboid migration, cells exhibit a rounded or ellipsoid morphology, weak cell–substrate adhesion, and no stress fibers but elevated cortical contractility. Distinct amoeboid motility modes have been described, depending on the leading edge structures (pseudopods, blebs, or single stable bleb; Friedl and Wolf, 2010; Liu *et al.*, 2015; Ruprecht *et al.*, 2015). Furthermore, the amoeboid motility mode has a higher velocity than the mesenchymal mode (Sanz-Moreno *et al.*, 2008; Tozluoğlu *et al.*, 2013). Cells can switch between migration modes, a process known as cell plasticity, allowing tumor cells to adapt to changing environments (e.g., changes in adhesion or confinement; Friedl and Wolf, 2010; Liu *et al.*, 2015; Ruprecht *et al.*, 2015). At the molecular level, mutual antagonism between Rac and Rho GTPases controls this switching: Rac signaling inhibits Rho/ROCK-driven amoeboid migration, whereas the Rho/ROCK signaling pathway suppresses Rac-driven mesenchymal movement. In melanoma cells, Rac inhibition of Rho activity requires its effector, WAVE2, whereas Rho inactivates Rac through activation of ARHGAP22, a Rac GTPase-activating protein (GAP; Sanz-Moreno *et al.*, 2008). Furthermore, FilGAP, which is closely related to ARHGAP22, has been implicated in mesenchymal-to-amoeboid transition in different cancer cell types (Ohta *et al.*, 2006; Saito *et al.*, 2012; Nakamura, 2013).

In this study, we used a 3D spheroid cell invasion assay in which multicellular spheroids are embedded in a collagen type I matrix—the main structural protein of the interstitial ECM—to analyze the migration behavior of a panel of RMS-derived cell lines. This system reproduced the higher invasive potential of ARMS than ERMS cells, as observed clinically. Of interest, we observed that during invasion through the collagen I matrix, most ARMS cell lines adopted a rounded shape, whereas ERMS cell lines acquired an elongated phenotype. This prompted us to analyze the relevance of the Rho/ROCK signaling pathway in the invasive potential of ARMS cells to get new insights into the molecular mechanisms responsible of ARMS aggressiveness.

RESULTS

ARMS-derived cell lines are highly invasive and adopt a rounded morphology during invasion through a type I collagen matrix

To identify mechanisms involved in ARMS aggressiveness, we first analyzed the migration behavior of a panel of ERMS- and ARMS-derived cell lines using a 3D spheroid cell invasion assay in which multicellular spheroids are embedded in a type I collagen matrix to mimic the in vivo environment (Thuault *et al.*, 2013). In this system, cell invasion through the matrix can be followed by phase-contrast microscopy over time. After 2 d, ARMS-derived cells evaded efficiently from the spheroid to colonize the surrounding matrix. Conversely, ERMS-derived cells (except for the CT-10 cell line) poorly colonized the matrix (Figure 1A and Supplemental Table S1). These differences persisted over time (unpublished data). This indicates that the 3D invasion assay reproduces the higher in vitro

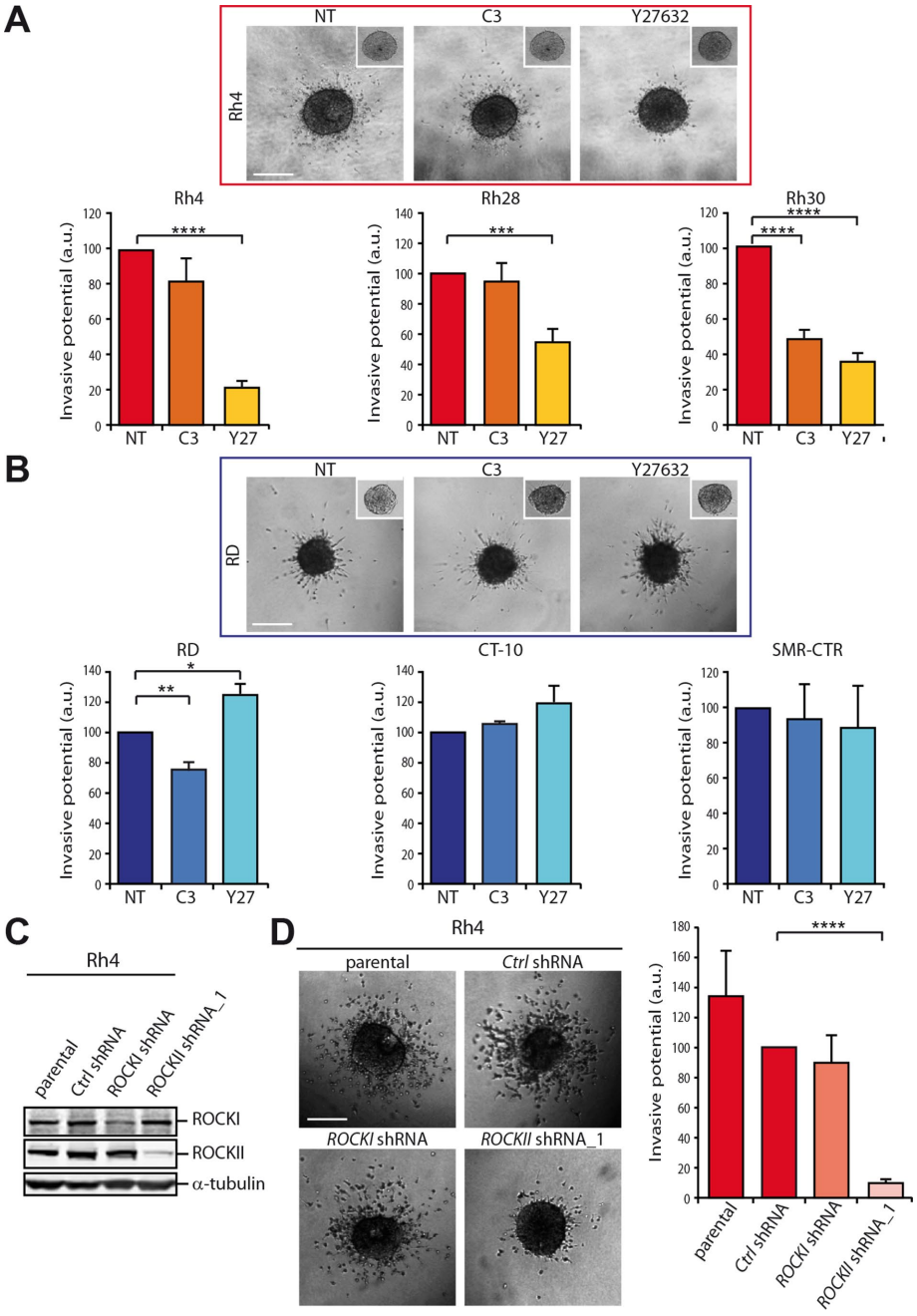

FIGURE 2: Invasion of ARMS-derived cells is ROCK dependent. Analysis of the invasive potential of ARMS (A) and ERMS (B) cell lines after incubation or not (NT) with 0.1 µg/ml exoenzyme C3 transferase (C3; Rho GTPase inhibitor) or 10 µM Y27632 (Y27; ROCK inhibitor) in a 3D spheroid cell invasion assay. Representative phase-contrast photographs of the invasion of Rh4 (ARMS) cells (A) and of RD (ERMS) cells (B) at day 2 after embedding in type I collagen. Insets, spheroids at day 0 just after embedding. The invasive potential is represented as the mean ± SEM of three independent experiments; nontreated cells (NT) were used as reference and set at 100%. (C) ROCKI and ROCKII expression in parental Rh4 (ARMS) cells and in Rh4 cells expressing control (*Ctrl* shRNA), anti-*ROCKI*, or anti-*ROCKII* shRNAs were assessed by Western blotting. α-Tubulin was used as loading control. (D) Analysis of the invasive potential of the Rh4 cell lines described in B using the 3D spheroid cell invasion assay. Phase-contrast images were taken at day 2 after embedding in type I collagen and are representative of at least 20 spheroids. The invasive potential is represented as the mean ± SEM of three independent experiments. *Ctrl* shRNA Rh4 cells were used as reference and set at 100%. *$p < 0.05$, **$p < 0.01$, ***$p < 0.001$, and ****$p < 0.0001$. Bar, 200 µm.

ARMS aggressiveness and is thus suitable for the identification of ARMS-specific pathways and ultimately of potential therapeutic targets (Wachtel and Schafer, 2010).

The precise analysis of the morphology of invading cells indicated that most invading ARMS cells had a round morphology (Figure 1A, insets of boxed regions). To better investigate this, we seeded different RMS cell lines on top of a thick layer of type I collagen, a system that recapitulates what happens in 3D matrices (Sahai and Marshall, 2003; Figure 1B). We found that most ARMS cell lines (Rh28, Rh4, Rh30, and SJ/Rh30) adopted a rounded, refractive morphology on the type I collagen matrix, whereas ERMS cell lines adopted an elongated, flattened mesenchymal morphology (Figure 1B). To quantify these morphological differences between ARMS and ERMS cell lines, we measured the perimeter and area of each cell and plotted the reciprocal of the circularity index (perimeter$^2/4\pi \times$ area; for round cells, this value is equal to 1). This value was ~2.5 for ERMS-derived RD cells, indicating that they adopted an elongated shape, whereas for ARMS-derived Rh4 cells, it was ~1.4, in agreement with their more rounded shape (Figure 1C). Analysis of cell morphology by imaging F-actin organization using confocal microscopy during invasion in the 3D invasion assay indicated that Rh5 cells (ARMS) mainly adopted a rounded, amoeboid morphology with blebs at their surface. Conversely, the few invading RD cells (ERMS) showed an elongated, mesenchymal morphology (Figure 1D). We thus conclude that ARMS and ERMS cell lines have different invasive potential and migration mode through collagen I matrix: ARMS cells are more invasive than ERMS cells, and ARMS cells adopt an ellipsoid amoeboid shape, whereas the few invading ERMS cells have an elongated mesenchymal morphology.

ARMS cell invasion is ROCK dependent

The rounded shape adopted by ARMS-derived cells when migrating through the 3D collagen I matrix led us to analyze the involvement of the Rho/ROCK signaling pathway, which was described as controlling amoeboid invasion (Sahai and Marshall, 2003; Sanz-Moreno *et al.*, 2008). First, we analyzed the effect of inhibiting this pathway on ARMS- and ERMS-derived cell invasion. The invasive potential of ARMS cells, but not of ERMS cells, was reduced upon inhibition of ROCK kinase activity by incubation with Y27632 (Y27; Figure 2, A and B) or H1152 (Supplemental Figure S1). Conversely, the invasive potential of the ERMS and ARMS (except for Rh30) cell lines was not, or only slightly, perturbed upon inhibition of Rho GTPases by incubation with exoenzyme C3 transferase (C3). To further address the role of ROCK kinase in the invasive potential of ARMS cells, we generated Rh4 cell lines that stably express

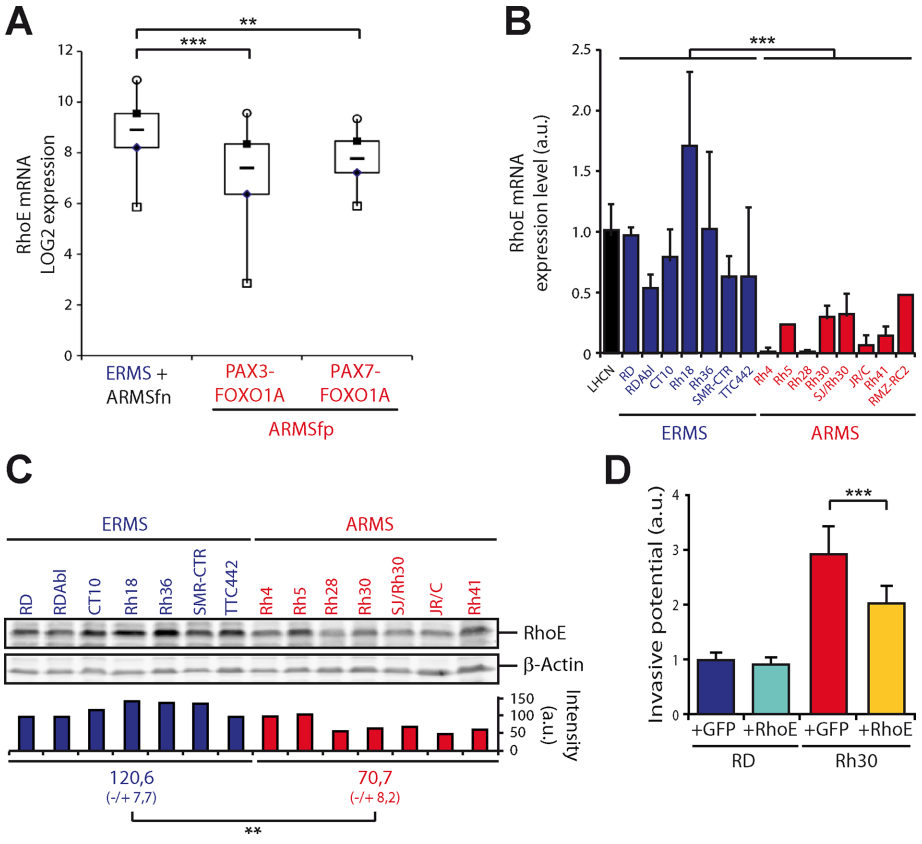

FIGURE 3: RhoE down-regulation in ARMS contributes to their invasive potential. (A) Box plot represents the normalized $\log_2$ intensity values of the probe set corresponding to RhoE in PAX-FOXO1A fusion-negative samples (i.e., ERMS and ARMSfn) and PAX3/7-FOXO1A fusion-positive ARMS samples (ARMSfp). (B) Quantification of *RhoE* mRNA expression by reverse transcription quantitative PCR (RT-qPCR) in RMS-derived cell lines. LHCN cells were used as reference and set to 1. Expression levels are presented as bar graphs of the mean value ± SD; $n = 3$. (C) RhoE expression assessed by Western blotting in RMS-derived cell lines. β-Actin was used as loading control. Quantification of the Western blotting. (D) Analysis of the invasive potential of RD (ERMS) and Rh30 (ARMS) cells infected with retroviruses expressing GFP or GFP fused to RhoE (GFP-RhoE) in Transwell cell culture chambers coated with a layer of Matrigel. The histogram shows the results of three independent experiments, each carried out in duplicate. Bars represent the SEM. $^{**}p < 0.01$, $^{***}p < 0.001$.

specific short hairpin RNAs (shRNAs) against *ROCKI* or *ROCKII*. Although the knockdown efficiencies were similar (Figure 2C), only ROCKII depletion strongly affected Rh4 cell invasion (Figure 2D). We obtained similar results with two independent shRNAs against ROCKII (Supplemental Figure S1B). These results demonstrate that ROCK activity is required for the invasive potential of ARMS but not ERMS cells, in agreement with the cell shape differences observed in the 3D spheroid cell invasion assay.

RhoE down-regulation in ARMS cells contributes to their high invasive potential

Analysis of ROCK kinase expression in a previously published microarray data set from 101 RMS biopsies (Williamson *et al.*, 2010) and in our panel of RMS cell lines did not show any significant difference in mRNA or protein expression levels between ERMS and ARMS cells (Supplemental Figure S2; unpublished data). This suggests that the differential ROCK dependence between ERMS and ARMS relies on the regulation of ROCK activation. Because Rho, an upstream ROCK activator, was not involved in the regulation of the invasive potential of ARMS cells (Figure 2A), we investigated the expression of the GTPase RhoE, a well-known inhibitor of ROCK kinase activity (Chardin, 2003). Analysis of the previously published microarray data set (Williamson *et al.*, 2010) showed that *RhoE* expression was down-regulated in ARMS biopsies compared with ERMS samples. Moreover, *RhoE* expression was specifically decreased in the most aggressive subtypes, those harboring the PAX3-FOXOA1 and PAX7-FOXOA1 fusion proteins (ARMSfp), compared with PAX3/7-FOXOA1 fusion-negative ARMS (ARMSfn) and ERMS biopsies (Figure 3A). Analysis of *RhoE* expression in three other microarray data sets (Wachtel *et al.*, 2004; Davicioni *et al.*, 2006; Laé *et al.*, 2007) confirmed this finding (unpublished data). We showed RhoE mRNA (Figure 3B) and protein (Figure 3C) down-regulation in our panel of ARMS cell lines (all harboring either the PAX3-FOXOA1 or the PAX7-FOXOA1 fusion protein) compared with the ERMS cell lines. To determine whether RhoE down-regulation could contribute to the invasive potential of ARMS cells, we overexpressed RhoE in ERMS-derived RD and ARMS-derived Rh30 cells (Figure 3D). RhoE overexpression reduced Rh30 cell invasion but had no effect on RD cells. These results suggest that low RhoE expression in ARMS cells contributes to their high invasive potential.

ARHGAP25 is highly expressed in ARMS cells and is required for their invasive potential

To address the role of the Rho GTPase signaling pathway in RMS development, we analyzed the expression of Rho GTPases and their regulators (guanine nucleotide exchange factors, GAPs, and guanine dissociation inhibitors) in the microarray data set published by Williamson *et al.* (2010). *ARHGAP25* was strongly up-regulated in both PAX3-FOXO1A and PAX7-FOXO1A fusion-positive ARMS compared with ERMS and PAX3/7-FOXO1A fusion-negative ARMS (ARMSfn; Figure 4A). Analysis of *ARHGAP25* expression in three other data sets (Wachtel *et al.*, 2004; Davicioni *et al.*, 2006; Laé *et al.*, 2007) confirmed this finding (unpublished data). Similarly, in RMS-derived cell lines, ARHGAP25 mRNA (Figure 4B) and protein (Figure 4C) were up-regulated only in PAX3/7-FOXO1A fusion-positive ARMS, showing that mRNA and protein levels are fully correlated. ARHGAP25 was never detected in control human myoblasts (LHCN-M2) and ERMS cell lines. Expression of ARHGAP22 and ARHGAP24, the two other family members, was not significantly different between ERMS and ARMS biopsies/cell lines (Supplemental Figure S3; unpublished data). These data suggest that ARHGAP25 could have a role in the invasive potential of ARMS cells. To test this hypothesis, we generated, by retroviral infection, stable ARMS-derived Rh4 cell lines that express specific shRNAs targeting ARHGAP25 (*ArhGAP25* shRNA_1 and *ArhGAP25* shRNA_2). Because ARHGAP25 expression in the cell pools was decreased by only 50% relative to the parental cell line or Rh4 cells expressing control shRNA (*Ctrl* shRNA; Figure 4D, *ArhGAP25* shRNA_1 pool), we selected independent clones with higher knockdown efficiency

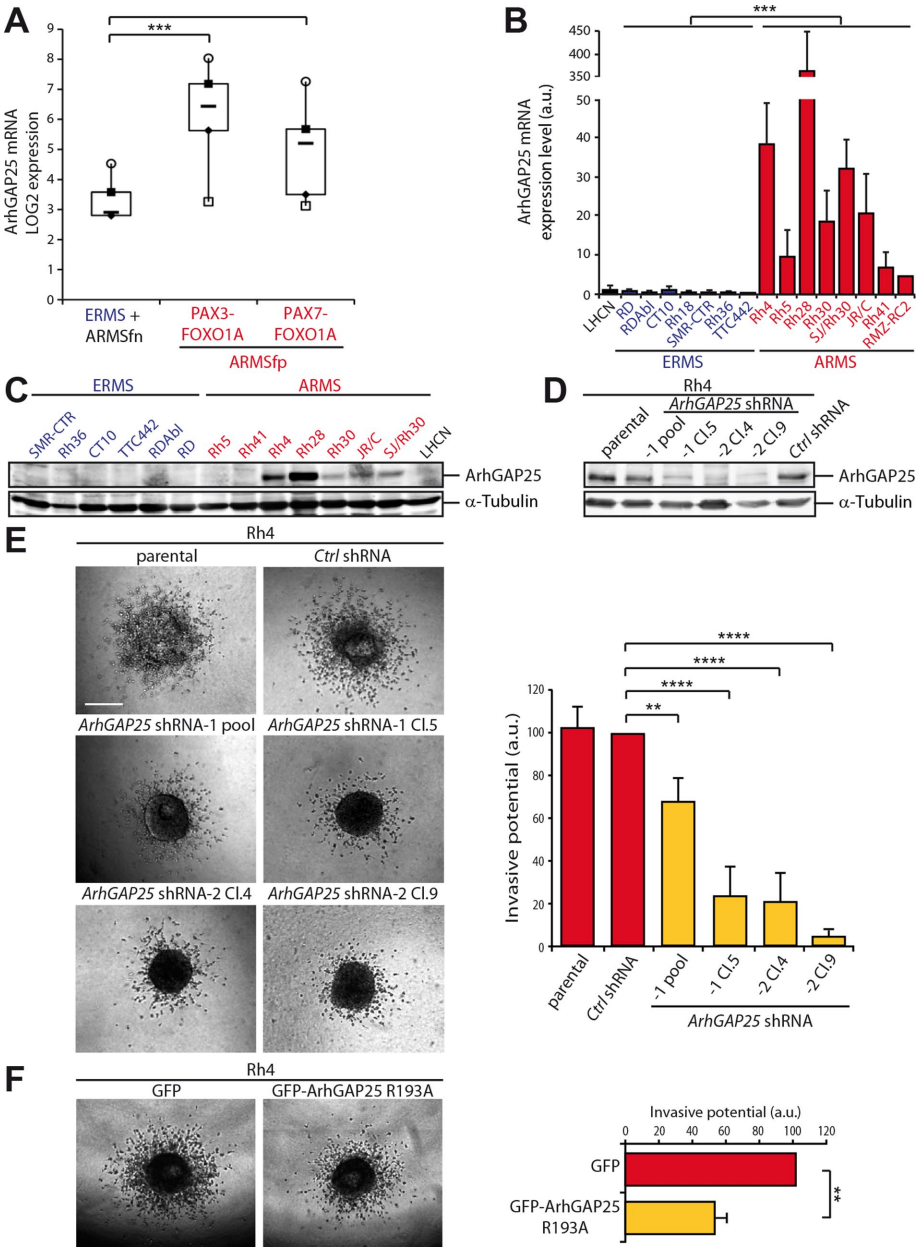

FIGURE 4: ARHGAP25 is highly expressed in PAX3-FOXO1A and PAX7-FOXO1A fusion-positive ARMS biopsies/cell lines and is required for their invasive potential. (A) Box plot represents the normalized $\log_2$ intensity values of the probe set corresponding to ARHGAP25 in PAX-FOXO1A fusion-negative samples (i.e., ERMS and ARMSfn) and PAX3/7-FOXO1A fusion-positive ARMS samples (ARMSfp). (B) Quantification of *ARHGAP25* mRNA level by RT-qPCR in RMS-derived cell lines. LHCN cells were used as reference and set to 1. Expression levels are presented as bar graphs of the mean values ± SD; $n = 3$. (C) ARHGAP25 expression assessed by Western blotting in RMS-derived cell lines. α-Tubulin was used as loading control. (D) ARHGAP25 expression in Rh4 (ARMS) cell pools or independent cell clones that express control shRNA (*Ctrl* shRNA) or specific shRNAs against *ARHGAP25* (*ARHGAP25* shRNA_1 and *ARHGAP25* shRNA_2) was assessed by Western blotting. α-Tubulin was used as loading control. (E) Analysis of the invasive potential of the Rh4-derived cells described in D using the 3D spheroid cell invasion assay. Images taken at day 2 after embedding in type I collagen are representative of at least 20 spheroids. Bar, 200 µm. The invasive potential is represented as the mean ± SEM of three independent experiments. *Ctrl* shRNA Rh4 cells were used as reference and set at 100%. (F) Analysis of the invasive potential (3D spheroid cell invasion assay) of Rh4 cells that express GFP alone or GFP-ARHGAP25R193A after selection of GFP-positive cells by FACS. Images were taken at day 2 after embedding in type I collagen and are representative of at least 20 spheroids. Bar, 200 µm. The invasive potential is represented as the mean ± SEM of three independent experiments. Rh4 cells that express GFP alone were used as reference and set at 100%. $^{**}p < 0.01$, $^{***}p < 0.001$, $^{****}p < 0.0001$.

(*ArhGAP25* shRNA_1 Cl.5, shRNA_2 Cl.4 and shRNA_2 Cl.9; Figure 4D). We then tested the invasive potential of these individual clones in the 3D spheroid cell invasion assay. Whereas parental and *Ctrl* shRNA cells efficiently invaded the type I collagen matrix, the invasive potential of *ARHGAP25* shRNA cells was decreased (Figure 4E), and this effect was correlated with *ARHGAP25* knockdown efficiency. Of interest, expression of an ARHGAP25 mutant (ARHGAP25R193A) without any GAP activity against Rac (see subsection) inhibited the invasive potential of Rh4 cells (Figure 4F). These results demonstrate that ARHGAP25 is required for the invasive potential of ARMS cells.

ROCK regulates Rac activity via ARHGAP25

ARHGAP25, like its close family member ARHGAP24 (FilGAP), is a GAP for Rac (Csepanyi-Komi *et al.*, 2012). To address this point in RMS cells, we first analyzed the effect of ARHGAP25 on the RMS cell ability to spread on poly-L-lysine–coated coverslips as a readout of Rac activity (Price *et al.*, 1998). Ectopic expression of wild-type ARHGAP25 (ArhGAP25 WT) in ERMS-derived RD cells, which do not express endogenous ARHGAP25, reduced their spreading. Conversely, expression of the catalytically inactive ARHGAP25R193A mutant did not have any effect, and these cells spread as efficiently as control cells (transfected with the empty vector pMXS; Figure 5A). On the other hand, overexpression of the ARHGAP25R193A mutant in ARMS-derived Rh4 cells, which express high levels of endogenous ARHGAP25, promoted cell spreading. This indicates that this mutant acts as a dominant negative toward endogenous ARHGAP25 (Figure 5B). Accordingly, measurement of Rac1 activity by pull-down assays showed that ARHGAP25R193A expression in Rh4 cells increased Rac1 activity (Figure 5C). These results confirmed that in RMS cells, ARHGAP25 is a GAP for Rac and that its catalytic activity is required for Rac activity inhibition.

It has been reported that ROCK kinases inhibit Rac activity via regulation of FilGAP (ARHGAP24) or ARHGAP22 activity, depending on the cell type (Ohta *et al.*, 2006; Sanz-Moreno *et al.*, 2008). We thus investigated whether in ARMS-derived cells Rac activity could be regulated by ROCKII via ARHGAP25. To this aim, we first analyzed the effect of ROCKII depletion on Rac activity. Rh4 cells in which *ROCKII* was silenced by shRNA spread more efficiently (Figure 5D) and displayed higher

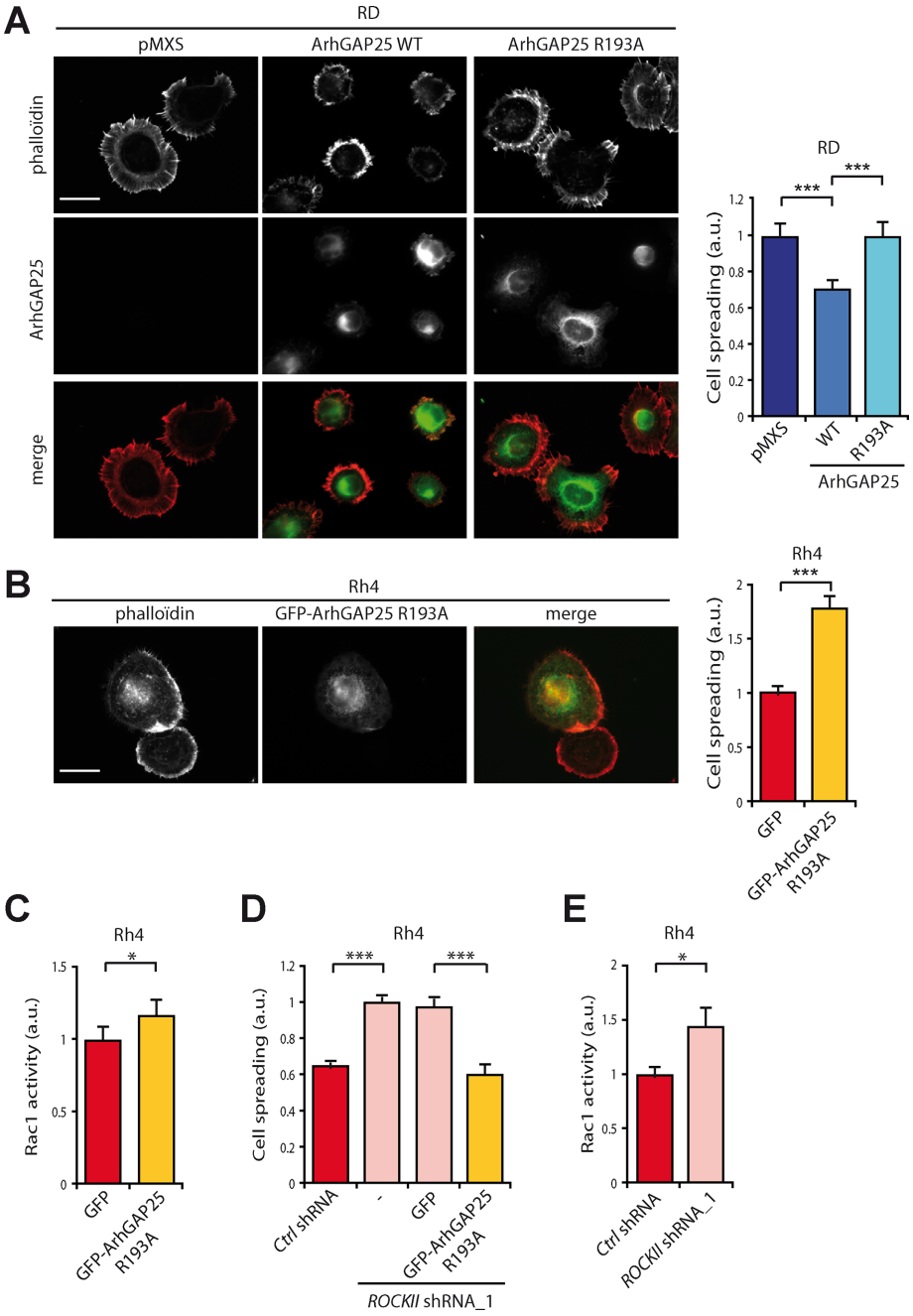

FIGURE 5: ROCKII regulates Rac activity via ARHGAP25. (A) Representative images of RD (ERMS) cells transiently transfected with empty vector (pMXS) or vectors expressing wild-type ARHGAP25 (WT) or the ARHGAP25 R193A mutant 30 min after plating on poly-L-lysine–coated coverslips. Cells were stained with an antibody against ARHGAP25 (green) and rhodamine-conjugated phalloidin (red). Bar, 10 µm. The histogram shows the quantification of cell spreading (mean cell area ± SEM; $n = 3$). ***$p < 0.001$. (B) Representative images of Rh4 (ARMS) cells transiently transfected with vectors expressing GFP alone or GFP-ARHGAP25 R193A 30 min after plating on poly-L-lysine–coated coverslips. Cells were stained with rhodamine-conjugated phalloidin. Bar, 10 µm. The histogram shows the quantification of cell spreading (mean cell area ± SEM; $n = 3$). ***$p < 0.001$. (C) Analysis of Rac1 activity in Rh4 (ARMS) cells that stably express GFP or GFP-ARHGAP25 R193A (mean ± SD; $n = 3$). *$p < 0.05$. (D) Histogram showing the spreading of Rh4 (ARMS) cells that stably express control shRNA (*Ctrl* shRNA) or a specific shRNA against *ROCKII* (*ROCKII* shRNA) and transiently transfected or not with vectors expressing GFP or GFP-ARHGAP25 R193A on coverslips coated with poly-L-lysine 30 min after plating (mean cell area ± SEM; $n = 3$). ***$p < 0.001$ (E) Analysis of Rac1 activity in Rh4 ARMS cells that stably express control shRNA (*Ctrl* shRNA) or a specific shRNA against *ROCKII* (*ROCKII* shRNA; mean ± SD; $n = 3$). *$p < 0.05$.

level of active Rac1 (Figure 5E). This indicates that ROCKII regulates Rac activity in ARMS-derived cells, as described in other cell systems. To determine whether the effect of ROCKII on Rac activity could be ARHGAP25 dependent, we overexpressed ARHGAP25 in *ROCKII*-silenced Rh4 cells. ARHGAP25 overexpression inhibited the increased spreading of ROCKII-depleted cells, leading to similar levels of spreading as in cells expressing control shRNA. Expression of green fluorescent protein (GFP) alone had no effect (Figure 5D). These results indicate that in ARMS-derived cells, ROCKII regulates Rac activity via ARHGAP25.

DISCUSSION

ARMS are highly malignant pediatric tumors with a poor prognosis and high metastasis occurrence. It is therefore of great importance to determine the molecular pathways implicated in their invasive potential and in metastasis formation. In this study, we used a 3D spheroid cell invasion assay that recapitulates ARMS aggressiveness in vitro. Indeed, ARMS-derived cell lines invaded a type I collagen matrix more efficiently than ERMS-derived cell lines (Figure 1). Furthermore, we observed that ARMS-derived cell lines adopted a rounded morphology, whereas ERMS-derived cell lines, which are less invasive, adopted a mesenchymal morphology (Figure 1). These observations agree with previous studies demonstrating that amoeboid shape is correlated with the aggressive phenotype of several cancer cell lines. Cancer cells with a rounded morphology are more prone to invasion (Sanz-Moreno *et al.*, 2008; de Toledo *et al.*, 2012; Hager *et al.*, 2012; Domingues *et al.*, 2014; Liu *et al.*, 2015), whereas cells converting from the amoeboid to the mesenchymal type of migration are less efficient in invading the surrounding matrix (Saito *et al.*, 2012; Shao *et al.*, 2014).

The amoeboid motility mode relies on a high cortical actomyosin contractility, regulated by the Rho/ROCK signaling pathway (Sahai and Marshall, 2003). Here we find that inhibition of ROCK kinases strongly reduces ARMS cell invasion, demonstrating that the aggressive phenotype of ARMS cells relies on actomyosin contractility. Although invasion of ARMS cells depends on ROCK (Figure 2), none of the three Rho GTPases (RhoA, RhoB, and RhoC) seems to be acting upstream of ROCK to regulate the invasive potential of ARMS cells, with the exception of Rh30 cells (Figure 2A). Indeed, ARMS cell invasion was not affected or only slightly so when Rho GTPases were inhibited by

incubation with exoenzyme C3 transferase. However, we found that the constitutively active GTPase RhoE/RND3 was down-regulated in PAX3/7-FOXO1A fusion-positive ARMS compared with ERMS and PAX3/7-FOXO1A fusion-negative biopsies. Moreover, RhoE overexpression inhibited ARMS but not ERMS cell invasion (Figure 3). RhoE is a well-known inhibitor of the Rho/ROCK signaling pathway and acts by inhibiting RhoA activity through inactivation of p190RhoGAP (Wennerberg *et al.*, 2003) or direct inactivation of ROCKI after its binding (Riento *et al.*, 2003). Because ARMS cell invasion was mostly independent of the three Rho GTPases, our results suggest that RhoE directly controls ROCK kinase activity, as reported in hepatocellular carcinoma (Grise *et al.*, 2012). Depending on the cell type, RhoE inhibits either ROCKI or ROCKII (Riento *et al.*, 2003; Grise *et al.*, 2012; Ma *et al.*, 2013). In ARMS cells, our results suggest that RhoE specifically inhibits ROCKII activity. However additional experiments are needed to dissect the underlying molecular mechanisms. Our findings demonstrate that ARMS aggressiveness relies on the RhoE/ROCK signaling. Of importance, in cancer cells, the balance between amoeboid and mesenchymal migration is regulated by proteins controlling Rac and Rho activities (Sanz-Moreno *et al.*, 2008). When we analyzed microarray data sets from RMS tumors to identify regulators of small Rho GTPase activities that are differentially expressed between ERMS and ARMS, we found that ARHGAP25 was up-regulated in PAX3/7-FOXO1A fusion-positive ARMS compared with ERMS and PAX3/7-FOXO1A fusion-negative biopsies (Figure 4). Moreover, ARHGAP25 is down-regulated after PAX3-FOXO1A knockdown (Ebauer *et al.*, 2007; Liu *et al.*, 2012). This is the first time that ARHGAP25 expression has been associated with cancer. Recently ARHGAP25 has been described to be specifically expressed in hematopoietic cells and to regulate phagocytosis (Csepanyi-Komi *et al.*, 2012; Schlam *et al.*, 2015). ARHGAP25 is a GAP for Rac and belongs to the same family as ARHGAP22 and ARHGAP24 (FilGAP; Csepanyi-Komi *et al.*, 2012). ARHGAP22 and ARHGAP24 are involved in mesenchymal-to-amoeboid transition by inhibiting Rac activity in different cancer cell types (Sanz-Moreno *et al.*, 2008; Saito *et al.*, 2012), and they are regulated by ROCK kinases. For instance, ROCK kinase–mediated phosphorylation of ARHGAP24 is required for its GAP activity (Ohta *et al.*, 2006). Whereas it was difficult to assess ROCK-dependent ARHGAP25 phosphorylation in ARMS cells, we observed that in ARMS, *ARHGAP25* expression was down-regulated upon stable ROCKII depletion (unpublished data).

Furthermore, we demonstrated that ARHGAP25 is required for ROCK regulation of Rac activity (Figure 5), as described for ARHGAP22 and ARHGAP24 (Ohta *et al.*, 2006; Sanz-Moreno *et al.*, 2008). However, in contrast to ARHGAP24 (Saito *et al.*, 2012), ARHGAP25 overexpression did not induce membrane blebbing, typical of ROCK kinase activation (unpublished data). This suggests that in ARMS cells, ARHGAP25 controls only Rac activity downstream of ROCK activation and not membrane blebbing. In agreement, we did not observe a classical amoeboid-to-mesenchymal transition after inhibition of ARHGAP25 activity.

Adhesion, 3D confinement, and cortical contractility control cell motility mode (Friedl and Wolf, 2010; Liu *et al.*, 2015; Ruprecht *et al.*, 2015). In this study, we used type I collagen to show that ARMS cells use an amoeboid invasion mode controlled by the RhoE/ROCK/ARHGAP25 signaling pathway. It would be interesting to use different matrices and 3D confinement to address how ARMS cells adapt to changing environments and how the signaling pathway highlighted here is implicated. In fact, we have preliminary data suggesting that ARMS motility can also depend on proteases (unpublished data). Matrix degradation by proteases has been correlated with mesenchymal motility, but recently it was also described as necessary for the amoeboid mode of invasion (Orgaz *et al.*, 2014). Further studies are required to address how ARMS cells can adapt to changing environments.

Overall, our study demonstrates that the RhoE/ROCK/ARHGAP25 signaling pathway controls the invasive potential of ARMS cells, and each of the constituents of this signaling cascade are therefore new potential therapeutic targets for ARMS.

MATERIALS AND METHODS

Microarray analysis

The HG-U133plus2.0 Affymetrix microarray data of RMS tumor samples were used for gene expression analyses (Williamson *et al.*, 2010). Box plots represent the normalized $\log_2$ intensity values of the probe sets corresponding to ARHGAP25 (probe sets 204882_at and 38149_at, HUGO gene symbol ARHGAP25) and RHOE (probe set 212724_at, HUGO gene symbol RND3) in the following sample groups: 1) ERMS and PAX3/7-FOXO1A fusion-negative ARMS (ARMSfn), 2) PAX3-FOXO1A, and 3) PAX7-FOXO1A fusion-positive ARMS (ARMSfp).

Cell lines

Culture conditions of LHCN-M2 human myoblasts and of ERMS- and ARMS-derived cell lines have been previously described (Thuault *et al.*, 2013).

Plasmid constructs

mRNA of Rh4 and Rh28 ARMS-derived cell lines was reverse transcribed with oligo(dT) and then PCR amplified with specific primers designed to amplify the four potential isoforms of human ARHGAP25 and containing the *Bam*HI and *Xho*I restriction sites for cloning in the pMXs-puro retroviral vector (Supplemental Table S2). The only ARHGAP25 isoform that could be amplified was isoform c (NM_001166276.1). To generate the GFP-ARHGAP25 fusion protein, ARHGAP25 was amplified by PCR using specific primers containing the *Xho*I and *Bam*HI restriction sites using pMXs-puro-ARHGAP25 as template and then cloned in pEGFP-C3 (Supplemental Table S2). Mutation of the critical arginine of the GAP domain (ARHGAP25 R193A) was performed using the QuikChange Site-Directed Mutagenesis Kit (Stratagene, Agilent Technologies, France) following the manufacturer's instructions (Supplemental Table S2).

shRNA constructs were made using the retroviral vector RNAi-ready pSIREN-RetroQ according to the manufacturer's protocol (Clontech, Ozyme, Saint-Quentin-en-Yvelines, France). The oligonucleotides used to suppress endogenous expression of ARHGAP25 (NM_001166276.1), ROCKI (NM_005406), and ROCKII (NM_004850) are listed in Supplemental Table S2. As control, we used the *Control* shRNA (*Ctrl* hRNA) provided with the RNAi-ready pSIREN-RetroQ kit. All constructs were checked by DNA sequencing.

Establishment of stable cell lines by retroviral infection

Retroviral infection was performed as described (Fortier *et al.*, 2008). Infected Rh4 cells were selected in medium containing 0.5 μg/ml puromycin. Independent cell clones were derived by limited dilution.

Establishment of stable cell lines after transfection

To establish cell lines expressing specific GFP fusion proteins, cells were transfected using the TransIT-LT1 transfection reagent (Mirus, Euromedex, Souffelweyersheim, France) according to manufacturer's instructions, selected in medium containing 1.75 mg/ml G418, and sorted by fluorescence-activated cell sorting (FACS), based on GFP expression (FACSAria), to obtain a high percentage of GFP-positive cells.

Quantitative real-time reverse transcription PCR

Total RNAs from cell lines were prepared as described in Fortier *et al*. (2008). Primers used are described in Supplemental Table S2. Human *TBP* mRNA was used as reference. The control condition was set to 1, and expression levels are presented as bar graphs of mean values ± SD.

Gel electrophoresis and immunoblotting

Proteins were extracted as described in Bach *et al*. (2010) and then resolved on polyacrylamide gels and transferred to Immobilon-P membranes. Membranes were then incubated with rabbit anti-ARHGAP25 (HPA035346; Sigma-Aldrich, Saint-Quentin Fallavier, France), mouse monoclonal anti-ROCK-I (611136; BD Biosciences, Le Pont de Claix, France), anti–ROCK-II (610623; BD Transduction Laboratories), anti-RhoE (05-723; Merck Millipore), anti–β-actin (A1978; Sigma-Aldrich), or anti–α-tubulin (A2066; Sigma-Aldrich) antibodies. Membranes were processed as described in Charrasse *et al*. (2002). For protein quantification, the Odyssey system from LI-COR Biosciences (Cambridge, United Kingdom) was used.

Transwell invasion assay

Transwell cell culture chambers containing fluorescence-blocking polycarbonate porous membrane inserts (pore size 0.8 μm; Fluoroblock; BD Biosciences) were coated with a thick layer of 0.3 mg/ml Matrigel (BD Biosciences). We plated 5×10^4 cells in DMEM containing 1% fetal calf serum (FCS) on top of the Matrigel. The lower chamber was filled with DMEM with 10% FCS to establish a soluble gradient of chemoattractant. Cells were allowed to invade at 37°C and 5% CO_2 for 24 h before fixation in 3.7% formaldehyde for 15 min. Cells that had invaded through the Matrigel were detected on the lower side of the filter by Hoechst staining and counted. Data are mean ± SD of at least three independent experiments.

Three-dimensional spheroid cell invasion assays

Semiconfluent cells were trypsinized and counted, and 10^4 cells/ml were resuspended in medium containing 2.4 mg/ml methylcellulose (Sigma-Aldrich). Then 100 μl of cell suspension was added in each well of a U-bottom 96-well plate, allowing the formation of one spheroid per well. All spheroids consisted of 10^3 cells. Two days after plating, spheroids were harvested and embedded into collagen. A flat-bottom 96-well-plate was coated with a 1:1 mix of a solution of neutralized bovine type I collagen (Purecol; Advanced BioMatrix, San Diego, CA) according to the manufacturer's protocol at 2.4 mg/ml and medium supplemented with 12 mg/ml methylcellulose. Single spheroids were embedded in a similar mix. Medium was added on top of the collagen. The ROCK inhibitors Y27632 (Calbiochem, Millipore, Molsheim, France) and H1152 (Tocris, R&D Bio-Techne, Lille, France) at a concentration of 10 μM and the exoenzyme C3 transferase of *Clostridium botulinum* (CT04; Cytoskeleton, ThermoFisher, France) at a concentration of 0.1 μg/ml were added to the coating, the embedding solution, and the medium on top of the collagen. Phase-contrast photographs were taken daily after embedding. The invasive potential was determined by calculating the mean number of cells invading further than an arbitrarily defined distance. Control conditions were set at 100%. Data are mean ± SEM of at least three independent experiments in which at least five spheroids were embedded per experimental condition.

Immunostaining of cells embedded in collagen

Collagen pieces containing cells were fixed in a solution containing 4% paraformaldehyde and 1% glutaraldehyde at room temperature for 2 h, washed three times with phosphate-buffered saline (PBS) at room temperature for 30 min, and permeabilized in PBS containing 3% bovine serum albumin (BSA) and 0.2% Tween at room temperature for 2 h. Pieces were then incubated with rhodamine-conjugated phalloidin for actin cytoskeleton staining and Hoechst for nuclear staining in PBS containing 3% BSA and 0.05% Tween at 4°C overnight. They were then washed three times with PBS/0.05% Tween at room temperature for 30 min and mounted using ProLong Gold Antifade (Invitrogen, Villebon sur Yvette, France). Cell morphology was analyzed by confocal microscopy, followed by 3D image reconstitution (Imaris, Bitplane, Zurich, Switzerland).

Cell culture on thick layers of collagen I

Bovine dermal collagen I (PureCol; Advanced BioMatrix) was prepared at 1.7 mg/ml in DMEM. After collagen gel polymerization, cells were seeded on top of collagen in medium containing 10% FCS and allowed to adhere for 24 h, and medium was changed to 1% serum for 24 h. Phase contrast images were taken.

Spreading assays

After trypsinization, cells were plated on coverslips coated with 0.001% poly-L-lysine (Sigma-Aldrich) or 0.1% fibronectin (Sigma-Aldrich) and fixed for the indicated time after plating.

Rac1 activity

Rac1 activity was assessed using the G-LISA Rac1 Activation Assay, luminescent format (BK126; Cytoskeleton), following the manufacturer's instructions.

Immunofluorescence

Cells were prepared as described in Bach *et al*. (2010). Primary antibodies were revealed with Alexa Fluor 488 or 546–conjugated goat anti-mouse or anti-rabbit immunoglobulin G (Molecular Probes, Interchim, Montluçon, France).

Statistical analysis

For experiments with $n > 30$, the Student's *t* test was used to assess statistical differences between experimental conditions. For experiments with $n < 30$, the nonparametric Mann–Whitney U test was used.

ACKNOWLEDGMENTS

We thank Vincent Mouly for LHCN-M2 human myoblasts. We also thank the Montpellier Imaging Facility. This work was supported by the Ligue Nationale contre le Cancer (Equipe labellisée), the Association pour la Recherche contre le Cancer (fellowship to M.F.), the Institut National contre le Cancer (fellowship to S.T.), the Institut National de la Santé et de la Recherche Médicale (C.G.-R.), and the Centre national de la Recherche Scientifique (F.C.).

REFERENCES

Bach AS, Enjalbert S, Comunale F, Bodin S, Vitale N, Charrasse S, Gauthier-Rouviere C (2010). ADP-ribosylation factor 6 regulates mammalian myoblast fusion through phospholipase D1 and phosphatidylinositol 4,5-bisphosphate signaling pathways. Mol Biol Cell 21, 2412–2424.

Barr FG (2001). Gene fusions involving PAX and FOX family members in alveolar rhabdomyosarcoma. Oncogene 20, 5736–5746.

Breneman JC, Lyden E, Pappo AS, Link MP, Anderson JR, Parham DM, Qualman SJ, Wharam MD, Donaldson SS, Maurer HM, *et al*. (2003). Prognostic factors and clinical outcomes in children and adolescents with metastatic rhabdomyosarcoma–a report from the Intergroup Rhabdomyosarcoma Study IV. J Clin Oncol 21, 78–84.

Chardin P (2003). GTPase regulation: getting aRnd Rock and Rho inhibition. Curr Biol 13, R702–R704.

Charrasse S, Meriane M, Comunale F, Blangy A, Gauthier-Rouviere C (2002). N-cadherin-dependent cell-cell contact regulates Rho GTPases and beta-catenin localization in mouse C2C12 myoblasts. J Cell Biol 158, 953–965.
Csepanyi-Komi R, Sirokmany G, Geiszt M, Ligeti E (2012). ARHGAP25, a novel Rac GTPase-activating protein, regulates phagocytosis in human neutrophilic granulocytes. Blood 119, 573–582.
Davicioni E, Finckenstein FG, Shahbazian V, Buckley JD, Triche TJ, Anderson MJ (2006). Identification of a PAX-FKHR gene expression signature that defines molecular classes and determines the prognosis of alveolar rhabdomyosarcomas. Cancer Res 66, 6936–6946.
de Toledo M, Anguille C, Roger L, Roux P, Gadea G (2012). Cooperative anti-invasive effect of Cdc42/Rac1 activation and ROCK inhibition in SW620 colorectal cancer cells with elevated blebbing activity. PLoS One 7, e48344.
Domingues MJ, Rambow F, Job B, Papon L, Liu W, Larue L, Bonaventure J (2014). β-Catenin inhibitor ICAT modulates the invasive motility of melanoma cells. Cancer Res 74, 1983–1995.
Ebauer M, Wachtel M, Niggli FK, Schafer BW (2007). Comparative expression profiling identifies an in vivo target gene signature with TFAP2B as a mediator of the survival function of PAX3/FKHR. Oncogene 26, 7267–7281.
Fortier M, Comunale F, Kucharczak J, Blangy A, Charrasse S, Gauthier-Rouviere C (2008). RhoE controls myoblast alignment prior fusion through RhoA and ROCK. Cell Death Differ 15, 1221–1231.
Friedl P, Alexander S (2011). Cancer invasion and the microenvironment: plasticity and reciprocity. Cell 147, 992–1009.
Friedl P, Wolf K (2010). Plasticity of cell migration: a multiscale tuning model. J Cell Biol 188, 11–19.
Grise F, Sena S, Bidaud-Meynard A, Baud J, Hiriart JB, Makki K, Dugot-Senant N, Staedel C, Bioulac-Sage P, Zucman-Rossi J, *et al.* (2012). Rnd3/RhoE Is down-regulated in hepatocellular carcinoma and controls cellular invasion. Hepatology 55, 1766–1775.
Hager MH, Morley S, Bielenberg DR, Gao S, Morello M, Holcomb IN, Liu W, Mouneimne G, Demichelis F, Kim J, *et al.* (2012). DIAPH3 governs the cellular transition to the amoeboid tumour phenotype. EMBO Mol Med 4, 743–760.
Laé M., Ahn E, Mercado G, Chuai S, Edgar M, Pawel B, Olshen A, Barr F, Ladanyi M (2007). Global gene expression profiling of PAX-FKHR fusion-positive alveolar and PAX-FKHR fusion-negative embryonal rhabdomyosarcomas. J Pathol 212, 143–151.
Liu L, Wang Y-D, Wu J, Cui J, Chen T (2012). Carnitine palmitoyltransferase 1A (CPT1A): a transcriptional target of PAX3-FKHR and mediates PAX3-FKHR–dependent motility in alveolar rhabdomyosarcoma cells. BMC Cancer 12, 154–154.
Liu Y-J, Le Berre M, Lautenschlaeger F, Maiuri P, Callan-Jones A, Heuzé M, Takaki T, Voituriez R, Piel M (2015). Confinement and low adhesion induce fast amoeboid migration of slow mesenchymal cells. Cell 160, 659–672.
Ma W, Wong CC, Tung EK, Wong CM, Ng IO (2013). RhoE is frequently down-regulated in hepatocellular carcinoma (HCC) and suppresses HCC invasion through antagonizing the Rho/Rho-kinase/myosin phosphatase target pathway. Hepatology 57, 152–161.
Merlino G, Helman LJ (1999). Rhabdomyosarcoma–working out the pathways. Oncogene 18, 5340–5348.
Nakamura F (2013). FilGAP and its close relatives: a mediator of Rho-Rac antagonism that regulates cell morphology and migration. Biochem J 453, 17–25.
Ohta Y, Hartwig JH, Stossel TP (2006). FilGAP, a Rho- and ROCK-regulated GAP for Rac binds filamin A to control actin remodelling. Nat Cell Biol 8, 803–814.
Orgaz JL, Pandya P, Dalmeida R, Karagiannis P, Sanchez-Laorden B, Viros A, Albrengues J, Nestle FO, Ridley AJ, Gaggioli C, *et al.* (2014). Diverse matrix metalloproteinase functions regulate cancer amoeboid migration. Nat Commun 5, 4255.
Price LS, Leng J, Schwartz MA, Bokoch GM (1998). Activation of Rac and Cdc42 by integrins mediates cell spreading. Mol Biol Cell 9, 1863–1871.
Riento K, Guasch RM, Garg R, Jin B, Ridley AJ (2003). RhoE binds to ROCK I and inhibits downstream signaling. Mol Cell Biol 23, 4219–4229.
Ruprecht V, Wieser S, Callan-Jones A, Smutny M, Morita H, Sako K, Barone V, Ritsch-Marte M, Sixt M, Voituriez R, *et al.* (2015). Cortical contractility triggers a stochastic switch to fast amoeboid cell motility. Cell 160, 673–685.
Sahai E, Marshall CJ (2003). Differing modes of tumour cell invasion have distinct requirements for Rho/ROCK signalling and extracellular proteolysis. Nat Cell Biol 5, 711–719.
Saito K, Ozawa Y, Hibino K, Ohta Y (2012). FilGAP, a Rho/Rho-associated protein kinase-regulated GTPase-activating protein for Rac, controls tumor cell migration. Mol Biol Cell 23, 4739–4750.
Sanz-Moreno V, Gadea G, Ahn J, Paterson H, Marra P, Pinner S, Sahai E, Marshall CJ (2008). Rac activation and inactivation control plasticity of tumor cell movement. Cell 135, 510–523.
Sanz-Moreno V, Marshall CJ (2010). The plasticity of cytoskeletal dynamics underlying neoplastic cell migration. Curr Opin Cell Biol 22, 690–696.
Schlam D, Bagshaw RD, Freeman SA, Collins RF, Pawson T, Fairn GD, Grinstein S (2015). Phosphoinositide 3-kinase enables phagocytosis of large particles by terminating actin assembly through Rac/Cdc42 GTPase-activating proteins. Nat Commun 6, 8623.
Shao H, Li S, Watkins SC, Wells A (2014). alpha-Actinin-4 is required for amoeboid-type invasiveness of melanoma cells. J Biol Chem 289, 32717–32728.
Sorensen PHB, Lynch JC, Qualman SJ, Tirabosco R, Lim JF, Maurer HM, Bridge JA, Crist WM, Triche TJ, Barr FG (2002). PAX3-FKHR and PAX7-FKHR gene fusions are prognostic indicators in alveolar rhabdomyosarcoma: a report from the children's oncology group. J Clin Oncol 20, 2672–2679.
Thuault S, Hayashi S, Lagirand-Cantaloube J, Plutoni C, Comunale F, Delattre O, Relaix F, Gauthier-Rouviere C (2013). P-cadherin is a direct PAX3-FOXO1A target involved in alveolar rhabdomyosarcoma aggressiveness. Oncogene 32, 1876–1887.
Tozluoğlu M, Tournier AL, Jenkins RP, Hooper S, Bates PA, Sahai E (2013). Matrix geometry determines optimal cancer cell migration strategy and modulates response to interventions. Nat Cell Biol 15, 751–762.
Wachtel M, Dettling M, Koscielniak E, Stegmaier S, Treuner J, Simon-Klingenstein K, Buhlmann P, Niggli FK, Schafer BW (2004). Gene expression signatures identify rhabdomyosarcoma subtypes and detect a novel t(2;2)(q35;p23) translocation fusing PAX3 to NCOA1. Cancer Res 64, 5539–5545.
Wachtel M, Schafer BW (2010). Targets for cancer therapy in childhood sarcomas. Cancer Treat Rev 36, 318–327.
Wennerberg K, Forget MA, Ellerbroek SM, Arthur WT, Burridge K, Settleman J, Der CJ, Hansen SH (2003). Rnd proteins function as RhoA antagonists by activating p190 RhoGAP. Curr Biol 13, 1106–1115.
Williamson D, Missiaglia E, de Reynies A, Pierron G, Thuille B, Palenzuela G, Thway K, Orbach D, Lae M, Freneaux P, *et al.* (2010). Fusion gene-negative alveolar rhabdomyosarcoma is clinically and molecularly indistinguishable from embryonal rhabdomyosarcoma. J Clin Oncol 28, 2151–2158.